



Optimized femtosecond laser direct-written fiber Bragg gratings with high reflectivity and low loss

JIAFENG WU,^{1,2} XIZHEN XU,^{1,2,*}  CHANGRUI LIAO,^{1,2}  XIAOYU WENG,¹  LIWEI LIU,¹ JUNLE QU,¹ YIPING WANG,^{1,2}  AND JUN HE^{1,2} 

¹Key Laboratory of Optoelectronic Devices and Systems of Ministry of Education/Guangdong Province, College of Physics and Optoelectronic Engineering, Shenzhen University, Shenzhen 518060, China

²Shenzhen Key Laboratory of Photonic Devices and Sensing Systems for Internet of Things, Guangdong and Hong Kong Joint Research Centre for Optical Fibre Sensors, Shenzhen University, Shenzhen 518060, China
*xizhenxu@szu.edu.cn

Abstract: We propose and experimentally demonstrate a femtosecond laser plane-by-plane (PI-b-PI) technology for inscription of high-quality fiber Bragg gratings (FBGs). The spherical aberration (SA) was introduced to elongate the focal volume, and then combined with the scanning process, an expanded rectangular refractive index modification (RIM) region can be achieved. Such RIM regions exhibit a length of 15 μm and a width of 14 μm . Note that it consists of a negative region and a positive region. We have systematically studied the influence of the overlap between the RIM region and fiber core on the spectrum of FBG. After optimizing, the core of a conventional single-mode fiber (SMF) is covered completely by using the positive RIM region, resulting in a significant enhancement of the coupling strength coefficient (i.e., 3177.6 m^{-1}). A 500 μm long FBG assembled by using these RIM regions can achieve a high reflectivity of 95.83%. Moreover, the cladding mode resonances in transmission spectrum are suppressed thoroughly, since the localized effect in RIM region was avoided. In addition, this FBG exhibits a high birefringence of 2.13×10^{-4} . Therefore, the proposed fabrication method can be used to inscribe high-quality FBGs that could be used in many fields such as communication, fiber laser, polarization-selective filtering and multi-parameter sensing.

© 2023 Optica Publishing Group under the terms of the [Optica Open Access Publishing Agreement](#)

1. Introduction

Fiber Bragg gratings (FBGs) as a significant optical fiber component are widely used in many fields, such as fiber laser, optical communication and optical fiber sensing. Studies on fabrication method of FBGs by using femtosecond laser have been widely reported, since high-quality FBGs can be directly inscribed in non-photosensitive fibers (i.e., pure silica fiber and sapphire fiber) by using this method. Mihailov *et al.* first reported on the inscription of FBGs by using femtosecond laser phase mask technology in 2003, and these FBGs exhibited high reflectivity and low out-of-band insertion loss. However, the cladding mode loss is nonnegligible [1]. Subsequently, they proposed laser beam scanning method to enlarge the refractive index modification (RIM) region, and the cladding mode loss was reduced effectively [2]. However, this phase mask technology is inflexible to create FBGs with various Bragg wavelengths by using only one phase mask. Moreover, it is not suitable for fabrication of the complex grating structures. Then femtosecond laser Talbot interferometry has been proposed, which is more versatile in the fabrication of a wavelength-division-multiplexed (WDM) FBGs array [3]. However, both high precision and high stability are required in the fabrication process due to the extremely short path difference in experimental setup (i.e., a few micrometers).

Femtosecond laser direct writing technology has been proposed, which consists of point-by-point (PbP) method and line-by-line (LbL) method. Assisted by the high numerical aperture (NA) objective and air-bearing three-dimensional translation stage, this method provides full flexibility in selecting the Bragg wavelength, order of the grating, and length of the grating [4,5]. However, FBGs induced by using this technology still have some shortcomings.

In case of PbP method, the limited RIM region induced by using a single pulse cannot cover the fiber core completely. This results in a relatively low overlap factor. Moreover, such RIM region would lead to localized effect, and then the strong cladding mode loss would occur [6,7]. To solve this problem, we fabricated FBGs in a small-core fiber, exhibiting the low cladding mode loss [8]. However, such special optical fibers fused with conventional single-mode fiber (SMF) would lead to a high loss due to mode field diameter mismatching. Moreover, PbP parallel-integrated FBGs were demonstrated to extend the RIM region, aiming to enhance the overlap factor [9]. But the cladding mode loss is still significant. Femtosecond laser beam shaping technologies, such as a cylindrical lens and a slit, were proposed to extend the width of RIM regions, meanwhile, filamentation process was demonstrated to elongate the length of RIM regions [10–13]. However, such RIM regions expanded in just one dimension could not completely cover the core of SMF, and hence the cladding mode loss still exists. Femtosecond laser LbL method has been proposed to induce a rectangular RIM region by means of multiple exposures, which is more potential to obtain the high-quality FBG [5]. A continuous core-scanning technique developed from LbL method was reported for inscription of FBGs, which exhibits a lower insertion loss of 0.1 dB and a higher Bragg resonance attenuation of 49 dB [14]. Due to the high NA of the objective, the Rayleigh length of the focal volume is merely several micrometers, which is lower than the diameter of fiber core (i.e., 10 μm). To solve this problem, multiple-layer LbL inscription was proposed to provide a 100% fiber core overlap. But this method is time-consuming (i.e., several hours for fabrication of only one FBG) [15].

In this paper, we demonstrated a femtosecond laser plane-by-plane (Pl-b-Pl) technology for inscription of FBGs with high reflectivity and low loss. A cover slip was used to introduce the spherical aberration (SA), benefiting for the elongation of the RIM region. Assisted by LbL scanning process, the rectangular RIM regions can be realized. Such a RIM region consists of a negative region and a positive region. We investigated the effect of focal position on the overlap between RIM region and fiber core. The results show that the positive regions were precisely inscribed into fiber and completely covered the fiber core, resulting in suppressive cladding mode coupling and enhanced coupling strength coefficient. Therefore, the proposed fabrication method can be used to inscribe high-quality FBGs that could be developed in many fields such as fiber laser, optical communication, fiber optical multi-parameter sensing and polarization-selective filtering.

2. Experimental setup for fabricating FBGs

As displayed in Fig. 1, the FBG is inscribed into the SMF (Corning SMF-28e) by the experimental setup. A frequency-doubled regenerative amplified Yb: KGW (KGd(WO₃)) femtosecond laser (Pharos, Light Conversion) with a central wavelength of 514 nm, a pulse width of 290 fs, a repetition rate of 200 kHz, and a spot diameter of 3.5 mm is employed. A pulse picker is employed to obtain various repetition rates. A motorized power attenuator and a polarization rotator are used to adjust the optical power and the polarization of the laser beam. An assembled 3D translation stage (Aerotech ABL15010, ANT130LZS, and ANT130V-5) is employed to move the fiber precisely. In our experiment, to study the effect of RIM region on the spectral characteristics of FBG, we selected two objectives, i.e., a dry objective (50 \times , NA = 0.42, Mitutoyo) and an oil-immersion objective (100 \times , NA = 1.25, Leica). In case the oil-immersion objective was used, the output face of the objective and the SMF were immersed in the index-matching oil ($n = 1.476$) to reduce the aberration at silica/air interfaces. The cover slip is not required in this process. In

case the dry objective was used, as shown in Fig. 1, the SMF was mounted on a fused silica plate and covered by a silica slip with a thickness of 0.13 mm. Another segment of SMF with the same diameter of 125 μm was also mounted on the silica plate. Two fibers are parallel and the incident laser beam could be perpendicular to the surface of the silica slip. Such a silica slip is an important element to introduce the SA, benefiting to increase the length of RIM regions [16]. Moreover, the index-matching oil was applied to fill the gap between these two fused silica plates. The cylindrical lens effect caused by the surface curvature of fiber could be eliminated. Subsequently, in the PbP process, as shown in the inset (a) of Fig. 1, the SMF was moved at a constant velocity precisely along fiber axis by using an assembled 3D translation stage. And the pitch of the grating is decided by the moving speed of 3D translation stage and the repetition rate of the laser. Note that the length of RIM regions inscribed by using oil-immersion objective was limited (i.e., $\sim 1 \mu\text{m}$), while the length could be extended to dozens of micrometers by using dry objective combined with the SA. In the PI-b-PI process, as shown in the inset (b) of Fig. 1, the SMF was moved precisely along the scanning trace, and then the grating pitch is dependent on the distance of trace. The rectangular RIM regions inscribed by using this method could cover 100% fiber core.

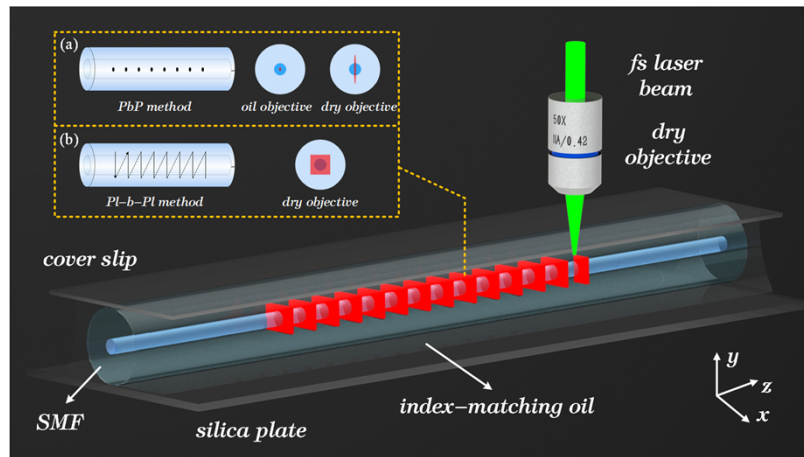


Fig. 1. Experimental setup for PI-b-PI FBG inscription with femtosecond laser. (Inset: (a) schematics of the PbP fabrication process and the cross-sections of the RIM formed by using oil-immersion objective and dry objective; (b) schematics of the PI-b-PI scanning process and the cross-section of the RIM formed by using dry objective.)

3. Experimental results and discussions

We study the effect of geometrical shape of RIM region on spectral characteristics of FBGs. A second-order FBG S1 with a grating pitch of 1.07 μm and a total length of 2 mm was inscribed into the fiber without coating by using PbP inscription method with the oil-immersion objective. The pulse energy was set as 70 nJ. As shown in Figs. 2(a1) and 2(b1), both the length and the width of RIM regions are 1 μm , respectively, which is smaller than the diameter of the fiber core (i.e., 10 μm). Figure 2(c1) shows that such RIM region is completely confined into the fiber core, resulting in a lower overlap with the mode field. As displayed in Fig. 2(d1), the transmission spectrum of this sample (S1) exhibits a Bragg resonance attenuation of 13.29 dB and an insertion loss of 1.16 dB, respectively. The coupling strength coefficient κ and the insertion loss coefficient α could be calculated as $\kappa = \ln(T_B)/(-2L)$ and $\alpha = \ln(T_{IL})/(-2L)$, where T_{IL} is the insertion loss, T_B is the Bragg resonance attenuation, and L is the length of grating [17]. The κ and α of FBG

S1 are 765.0 m^{-1} and 66.7 m^{-1} , respectively. And the ratio of κ/α could be calculated as 11.4. Moreover, note that the cladding mode resonances are significant, for example, the resonance attenuation at the wavelength of 1525 nm achieves 7.27 dB, resulting from the localized RIM region. When FBG was immersed into the index-matching oil ($n = 1.476$), a smooth transmission profile could be found in the range of short wavelength as coupling between the core mode to the continuum of radiation mode [18]. However, a cladding mode loss is still 4.18 dB, which is not conducive to the fabrication of chirped FBGs and WDM FBGs array. These results demonstrate that PbP FBGs created by using oil-immersion objective exhibit a lower ratio of κ/α and strong cladding mode resonances.

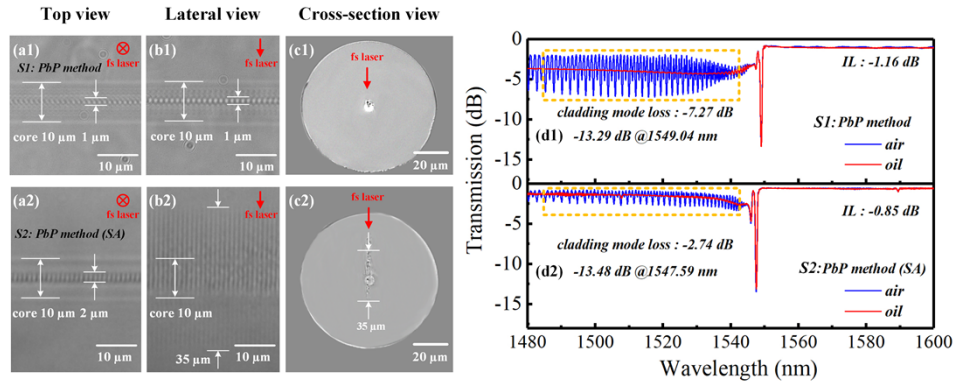


Fig. 2. A PbP FBG S1 inscribed by using oil-immersion objective and a PbP FBG S2 inscribed by using dry objective. (a) Top view microscope images, (b) lateral view microscope images, (c) cross-section view microscope images and (d) transmission spectra.

In order to solve this issue, the SA was employed to elongate the RIM regions. A second-order FBG S2 with a grating pitch of $1.07 \mu\text{m}$ and a total length of 2 mm was inscribed by using a PbP method with the dry objective assisted by a cover slip. A pulse energy of $7.5 \mu\text{J}$ was employed. Figures 2(a2) and 2(b2) show that the length and the width of the RIM regions are measured as $35 \mu\text{m}$ and $2 \mu\text{m}$, respectively. The RIM regions completely traverse the whole section of the fiber core with a diameter of $10 \mu\text{m}$, as illustrated in Fig. 2(c2), leading to the enhancement in the overlap with the mode field. As shown in Fig. 2(d2), compared with FBG S1, the transmission spectrum of this sample (S2) exhibits a similar resonance attenuation of 13.48 dB and a reduced insertion loss of 0.85 dB, respectively. The reason for this phenomenon is when the overlap factor increases, a higher coupling coefficient could be obtained by introducing a lower refractive index modulation, which means that a lower structural damage induced in fiber core was required. And hence, the insertion loss could be reduced [17,19]. The reflectivity of this sample (S2) is 95.51% and the ratio of κ/α could be calculated as 15.8, which is larger than the value of PbP FBG S1 fabricated by using oil-immersion objective. Moreover, the cladding mode resonances in transmission spectrum of FBG S2 decrease obviously, for example, the resonance attenuation at the wavelength of 1525 nm is 2.74 dB. When the FBG was immersed in index-matching oil ($n = 1.476$), the cladding mode loss is 1.53 dB. The reason for this phenomenon is that these needed-shaped RIM regions are elongated only in one dimension, which is still difficult to cover the whole fiber core.

In order to suppress the cladding mode resonance completely, the RIM regions require to cover the whole fiber core. And hence, we proposed LbL scanning technology combined with the dry objective to induce a PI-b-PI FBG. In the fabrication process, the pulse energy, the repetition rate and the writing speed were set as 80 nJ, 80 kHz and 0.2 mm/s, respectively. As shown in Figs. 3(a) and 3(b), a rectangular RIM region exhibits a width of $14 \mu\text{m}$ and a length of $15 \mu\text{m}$,

which is quite sufficient to cover the whole fiber core. Such an enlarged RIM region could be constructed, benefiting from LbL scanning technology and the SA. However, as shown in Fig. 3(c), the RIM region is not uniform, consisting of dark zone and bright zone. The refractive index difference of this RIM region was measured by using digital holographic microscopy (SHR-1602, Shanghai University, China). As displayed in Fig. 3(d), the measured result demonstrates that the refractive index changes in the dark zone and the bright zone are negative and positive, respectively. The reason for this phenomenon is that the nonlinear absorption process occurred when the femtosecond laser was focused into the fiber core. Then, the void was formed, indicating the decrease in the density of materials. That results in the negative refractive index change. Moreover, an instant thermo-mechanical expansion of the material and propagation of pressure wave occurred in the femtosecond laser beam focal volume. And the material within the black zone is thought to be pushed into the bright zone, forming the densified region. That leads to the positive refractive index change [20].

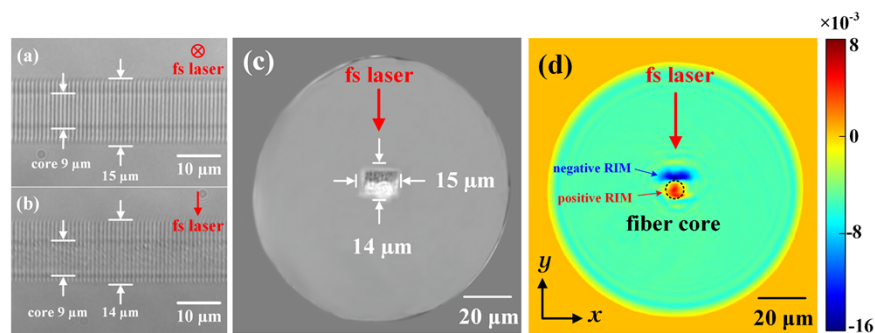


Fig. 3. A FBG inscribed by using PI-b-PI scanning process. (a) Top view microscope images, (b) lateral view microscope images, (c) cross-section view microscope images and (d) refractive index distribution in the cross section.

Subsequently, the effects of the relative location of RIM region in the fiber core on the spectra of FBGs were studied. Three second-order FBGs (S3-S5) with a grating length of 500 μm were inscribed at various focal depths by using femtosecond laser PI-b-PI method. In the fabrication process of FBG S3, the focus of the incident laser was 3 μm below the center of the fiber core. As shown in Figs. 4(a1)-(c1), the negative region occupies almost the whole fiber core. The transmission spectrum of FBG S3 exhibits a significant insertion loss of 2.29 dB, since the negative refractive index region located in the fiber core will hamper the transmission performance of the fiber core. Moreover, two transmission dips could be observed in the wavelength of 1548.44 nm and 1550.76 nm, and they exhibit the resonance attenuation of 5.01 dB and 2.01 dB, respectively. These two Bragg wavelengths correspond to the negative zone and the positive zone. Note that the transmission spectrum of FBG immersed in index-matching oil was coincident with that of FBG exposed to the air, which demonstrates that the cladding mode resonance could be suppressed completely. The benefits from the PI-b-PI method could be used to create the enlarged RIM region which is enough to cover the fiber core. In the fabrication process of FBG S4, the incident laser was focused in the center of the fiber core. As shown in Figs. 4(a2) and 4(b2), the negative region and the positive region occupy the part of fiber core, respectively. It can be observed that the overlap between the positive region and the fiber core is larger, resulting in a higher coupling strength coefficient in positive region. As shown in Fig. 4(c2), the transmission dip at Bragg wavelength of 1552.24 nm, corresponding to the positive region, exhibits a higher resonance attenuation of 11.88 dB. And the dip at Bragg wavelength of 1548.42 nm, corresponding to the negative region, exhibits a lower resonance attenuation of 5.68 dB. Moreover, the insertion loss decreases to 1.28 dB. In the fabrication process of FBG S5, the focus of the incident laser was

3 μm above the center of the fiber core. As shown in Figs. 4(a3) and 4(b3), the fiber core was occupied with the positive region. As displayed in Fig. 4(c3), only one dip at Bragg wavelength of 1553.10 nm with a higher resonance attenuation of 13.80 dB (i.e., reflectivity of 95.83%) could be observed. And the insertion loss decreases to 0.81 dB. The κ and α of FBG S5 could be calculated as 3177.6 m^{-1} and 186.5 m^{-1} , respectively. And the ratio of κ/α in S5 is 17.1, which is higher than that of FBG fabricated by PbP method. Notably, FBG S5 with a shorter grating length of 500 μm has the similar grating strength of FBG S2 with a grating length of 2 mm. It should be noted that the negative region is still close to the fiber core, as shown in Fig. 4(b3), and hence, increasing the grating length will lead to the nonnegligible insertion loss. Moreover, the cladding mode resonances are eliminated. However, it can be seen that a ghost mode with a loss of 4 dB still exists since a large gradient refractive index change at the interface of fiber core and cladding leads to the coupling from the core mode into LP_{11} i.e., ghost mode [2].

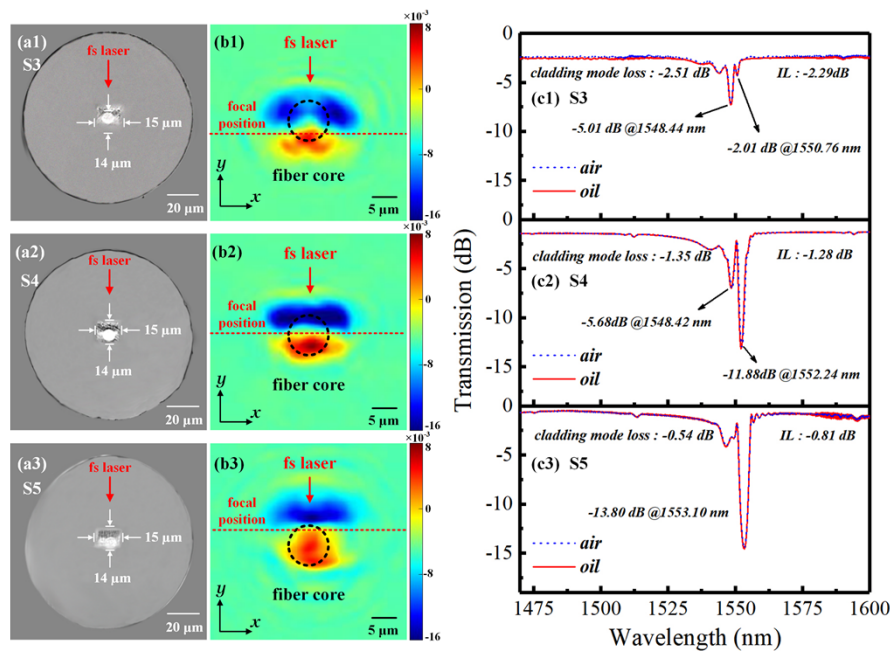


Fig. 4. The FBGs S3-S5 inscribed by using PI-b-PI scanning process. (a) Cross-section view microscope images, (b) refractive index distributions in the cross section and (c) transmission spectra.

Furthermore, the polarization-resolved transmission spectra and PDL spectra of FBG S1, FBG S2, and FBG S5 were measured by using a Muller-matrix-based commercial polarization analysis system, which consists of a tunable laser (Agilent, 81940A), a polarization synthesizer (Agilent, N7786B), and an optical power meter (Agilent, N7744A). The birefringence Δn_B can be calculated from $\Delta n_B = \Delta\lambda/\lambda$, where λ is the grating pitch, $\Delta\lambda$ is the Bragg wavelength difference between two orthogonal linear polarization modes (i.e., TE and TM) [21]. As shown in Fig. 5(a), the PbP FBG S1 inscribed by using oil-immersion objective exhibits a birefringence of 7.38×10^{-5} and a maximum PDL of 3.97 dB due to the elliptical cross-sectional pattern of RIM region created in the fiber core [11]. Moreover, the PbP FBG S2 inscribed by using dry objective exhibits a higher birefringence of 1.57×10^{-4} and a maximum PDL of 7.47 dB caused by the asymmetric needle-shaped RIM region, as shown in Fig. 2(c2). Note that the FBG S5 exhibits a birefringence of 2.13×10^{-4} and a maximum PDL of 2.84 dB. Such a higher birefringence results from the significant inhomogeneous effective refractive index distribution, which is induced by

the negative refractive index region closed to the fiber core, as shown in Fig. 4(b3). Therefore, the PI-b-PI FBG created by our method with a higher birefringence presents several assets, such as polarization-selective filtering capabilities and additional sensing modalities.

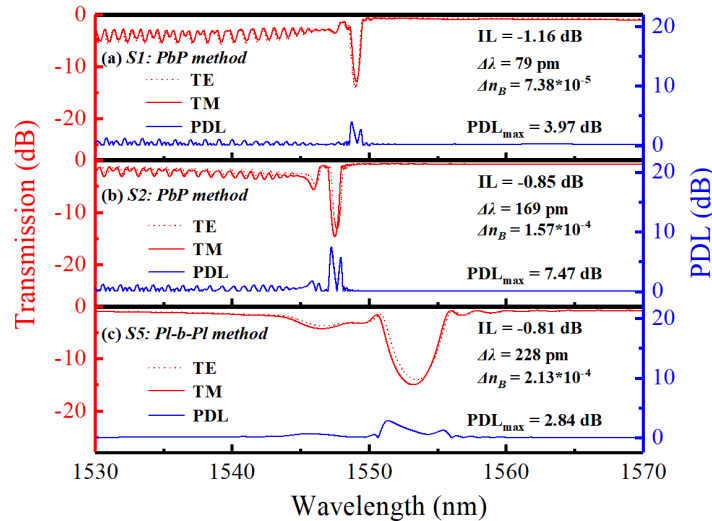


Fig. 5. Transmission spectra of two orthogonal linear polarization modes (i.e., TE and TM) and PDL spectra of (a) FBG S1 inscribed by using oil-immersion objective, (b) FBG S2 inscribed by using dry objective and (c) FBG S5 inscribed by PI-b-PI scanning process.

4. Conclusion

We have characterized the effect of geometrical shape of RIM region on spectral characteristics of FBGs. The FBGs inscribed by using the PbP method exhibit lower coupling strength coefficient and strong cladding mode resonance, resulting from the localized RIM region. We proposed the LbL scanning technology combined with the SA effect to induce a PI-b-PI FBG. The RIM region induced by using this method exhibits a length of 15 μm and a width of 14 μm . Note that such RIM region consists of a positive region and a negative region. The positive zone in RIM regions was precisely inscribed into the core, and then the FBG with a significantly enhanced coupling strength coefficient of 3177.6 m^{-1} and suppressive cladding mode resonance could be realized. Moreover, this FBG exhibits a high birefringence of 2.13×10^{-4} . As such, the proposed femtosecond laser PI-b-PI technology is a promising fabrication for high-quality FBG that could be developed in many fields such as communication, fiber laser, polarization-selective filtering and multi-parameter sensing.

Funding. National Natural Science Foundation of China (62222510, U1913212, 62005170); Department of Science and Technology of Guangdong Province (2022B1515120050, 2019TQ05X113); Science and Technology Innovation Commission of Shenzhen (RCYX20200714114538160, JCYJ20200109114201731, 20220810164735001).

Disclosures. The authors declare no conflicts of interest.

Data availability. Data underlying the results presented in this paper are not publicly available at this time but may be obtained from the authors upon reasonable request.

References

1. S. J. Mihailov, C. W. Smelser, P. Lu, R. B. Walker, D. Grobnic, H. M. Ding, G. Henderson, and J. Unruh, "Fiber Bragg gratings made with a phase mask and 800-nm femtosecond radiation," *Opt. Lett.* **28**(12), 995–997 (2003).
2. D. Grobnic, C. W. Smelser, S. J. Mihailov, R. B. Walker, and P. Lu, "Fiber Bragg gratings with suppressed cladding modes made in SMF-28 with a femtosecond IR laser and a phase mask," *IEEE Photonics Technol. Lett.* **16**(8), 1864–1866 (2004).

3. M. Becker, J. Bergmann, S. Brückner, M. Franke, E. Lindner, M. W. Rothhardt, and H. Bartelt, "Fiber Bragg grating inscription combining DUV sub-picosecond laser pulses and two-beam interferometry," *Opt. Express* **16**(23), 19169–19178 (2008).
4. A. Martinez, M. Dubov, I. Khrushchev, and I. Bennion, "Direct writing of fibre Bragg gratings by femtosecond laser," *Electron. Lett.* **40**(19), 1170–1172 (2004).
5. K. M. Zhou, M. Dubov, C. B. Mou, L. Zhang, V. K. Mezentsev, and I. Bennion, "Line-by-line fiber Bragg grating made by femtosecond laser," *IEEE Photonics Technol. Lett.* **22**(16), 1190–1192 (2010).
6. J. Thomas, N. Jovanovic, R. G. Becker, G. D. Marshall, M. J. Withford, A. Tünnermann, S. Nolte, and M. J. Steel, "Cladding mode coupling in highly localized fiber Bragg gratings: modal properties and transmission spectra," *Opt. Express* **19**(1), 325–341 (2011).
7. J. U. Thomas, N. Jovanovic, R. G. Krämer, G. D. Marshall, M. J. Withford, A. Tünnermann, S. Nolte, and M. J. Steel, "Cladding mode coupling in highly localized fiber Bragg gratings II: complete vectorial analysis," *Opt. Express* **20**(19), 21434–21449 (2012).
8. X. Y. Liu, Y. P. Wang, Z. L. Li, S. Liu, Y. Wang, C. L. Fu, C. R. Liao, Z. Y. Bai, J. He, Z. Y. Li, and L. P. Shao, "Low short-wavelength loss fiber Bragg gratings inscribed in a small-core fiber by femtosecond laser point-by-point technology," *Opt. Lett.* **44**(21), 5121–5124 (2019).
9. Y. P. Wang, Z. L. Li, S. Liu, C. L. Fu, Z. Y. Li, Z. Zhang, Y. Wang, J. He, Z. Y. Bai, and C. R. Liao, "Parallel-integrated fiber Bragg gratings inscribed by femtosecond laser point-by-point technology," *J. Lightwave Technol.* **37**(10), 2185–2193 (2019).
10. P. Roldan-Varona, D. Pallarés-Aldeiturriaga, L. Rodríguez-Cobo, and J. Miguel López-Higuera, "Slit beam shaping technique for femtosecond laser inscription of enhanced plane-by-plane FBGs," *J. Lightwave Technol.* **38**(16), 4526–4532 (2020).
11. X. Z. Xu, J. He, J. He, B. J. Xu, R. X. Chen, K. M. Yang, C. R. Liao, Y. T. Yang, and Y. P. Wang, "Slit beam shaping for femtosecond laser point-by-point inscription of high-quality fiber Bragg gratings," *J. Lightwave Technol.* **39**(15), 5142–5148 (2021).
12. P. Lu, S. J. Mihailov, H. M. Ding, D. Grobnc, R. B. Walker, D. Coulas, C. Hnatovsky, and A. Y. Naumov, "Plane-by-plane inscription of grating structures in optical fibers," *J. Lightwave Technol.* **36**(4), 926–931 (2018).
13. E. Ertorer, M. Haque, J. Z. Li, and P. R. Herman, "Femtosecond laser filaments for rapid and flexible writing of fiber Bragg grating," *Opt. Express* **26**(7), 9323–9331 (2018).
14. R. J. Williams, R. G. Krämer, S. Nolte, and M. J. Withford, "Femtosecond direct-writing of low-loss fiber Bragg gratings using a continuous core-scanning technique," *Opt. Lett.* **38**(11), 1918–1920 (2013).
15. G. Bharathan, T. T. Fernandez, M. Ams, R. I. Woodward, D. D. Hudson, and A. Fuerbach, "Optimized laser-written ZBLAN fiber Bragg gratings with high reflectivity and low loss," *Opt. Lett.* **44**(2), 423–426 (2019).
16. Q. Sun, H. B. Jiang, Y. Liu, Y. H. Zhou, H. Yang, and Q. H. Gong, "Effect of spherical aberration on the propagation of a tightly focused femtosecond laser pulse inside fused silica," *J. Opt. A: Pure Appl. Opt.* **7**(11), 655–659 (2005).
17. R. J. Williams, N. Jovanovic, G. D. Marshall, G. N. Smith, M. J. Steel, and M. J. Withford, "Optimizing the net reflectivity of point-by-point fiber Bragg gratings: the role of scattering loss," *Opt. Express* **20**(12), 13451–13456 (2012).
18. T. Erdogan, "Fiber grating spectra," *J. Lightwave Technol.* **15**(8), 1277–1294 (1997).
19. K. O. Hill and G. Meltz, "Fiber Bragg grating technology fundamentals and overview," *J. Lightwave Technol.* **15**(8), 1263–1276 (1997).
20. D. Z. Tan, X. Y. Sun, and J. R. Qiu, "Femtosecond laser writing low-loss waveguides in silica glass: highly symmetrical mode field and mechanism of refractive index change," *Opt. Mater. Express* **11**(3), 848–857 (2021).
21. N. Jovanovic, J. Thomas, R. J. Williams, M. J. Steel, G. D. Marshall, A. Fuerbach, S. Nolte, A. Tünnermann, and M. J. Withford, "Polarization-dependent effects in point-by-point fiber Bragg gratings enable simple, linearly polarized fiber lasers," *Opt. Express* **17**(8), 6082–6095 (2009).